

Hindered segmental dynamics in associative protein hydrogels studied by neutron spin-echo spectroscopy

Ameya Rao , Brian R. Carrick, Helen Yao, and Bradley D. Olsen **Department of Chemical Engineering, Massachusetts Institute of Technology, Cambridge, Massachusetts 02139, USA*

(Received 18 November 2022; revised 5 May 2023; accepted 10 May 2023; published 26 July 2023)

Transient binding between associating macromolecules can cause qualitative changes to chain dynamics, including modes of conformational relaxation and diffusion, through tethering effects imparted by long-range connectivity. In this work, the role of binding on short-time segmental dynamics in associative polymer gels is investigated by neutron spin-echo (NSE) measurements on a class of model artificial coiled-coil proteins with a systematically varied architecture, probing timescales of 0.1–130 ns, and length scales close to the molecular radius of gyration. The results illustrate effects of transient cross-linking on chain dynamics on different timescales, manifested in changes in segmental relaxation behavior with variations in strand length, chain concentration, and sticker distribution (endblock- vs midblock-functionalized). In all gels, a short-time cooperative diffusion mode is seen over all wave vectors, analogous to a semidilute solution, with no transitions seen at any known structural length scale. However, the diffusion coefficients are found to decrease with increasing junction density across all gels, with the strand length and number of stickers per chain in each gel appearing to play a relatively minor role. The slowing of cooperative diffusion with junction density contrasts with classical predictions of a greater restoring force for fluctuation dissipation due to the increased elasticity, suggesting additional effects of the coiled-coil junctions such as an enhancement in local viscosity that slows dynamics. Notably, the relaxation rates for all gels can be rescaled by the interjunction spacing inferred from small-angle neutron scattering, where they collapse onto a master curve suggestive of self-similar dynamics even in networks with different strand lengths and chain architectures. On long timescales (but shorter than the junction exchange time), a slowing of network relaxation is observed, resulting in a nondecaying plateau in the spin-echo amplitude attributed to a freezing of chain dynamics due to tethering. A characteristic length scale corresponding to the extent of dynamic fluctuations is estimated for each gel, which appears to be smaller than the interjunction spacing but similar to the correlation blob size of the overlapping strands. The results indicate an important role of transient binding on molecular-scale dynamics in associative polymer gels, even on timescales shorter than the junction exchange time, in addition to its effects on long-range self-diffusion previously observed.

DOI: [10.1103/PhysRevMaterials.7.075602](https://doi.org/10.1103/PhysRevMaterials.7.075602)

I. INTRODUCTION

Associative networks are pervasive in natural and synthetic macromolecular systems [1,2], serving important roles in processes ranging from selective transport in biophysical systems [3,4] to self-healing in soft materials [5,6]. Transient binding between macromolecules in solution can give rise to space-spanning three-dimensional networks with viscoelastic behavior dictated by the dynamics of the cross-links. Over the past few decades, extensive experimental [6–16] and theoretical [17–21] work has demonstrated a broad hierarchy of relaxation processes in transient networks, ranging from local conformational rearrangement of molecular subdomains to long-range self-diffusion of the polymer chains governed by repeated association and dissociation from the network structure [22]. These processes impart physical networks and gels with diverse properties including enhanced toughness and stimuli responsiveness and enable a large design

space including the molecular architecture, binding group distribution, and binding/unbinding kinetics [11,23–25].

While studies on associative networks have largely focused on their bulk viscoelasticity in the mean-field limit [17,19,26–28], the effect of physical associations on dynamics on length scales closer to the network mesh size remains less explored. Recent experiments and simulations have established a complex relationship between a molecule's sticker association configuration and its mechanisms of self-diffusion within the network, leading to unexpected dynamics not captured by mean-field theory [7,11,22,23,29,30]. In particular, anomalous diffusive behavior on length scales ~ 1 –100 times the radius of gyration has been attributed to an interplay between distinct dynamic modes governed by a molecule's connectivity to the network, establishing the important role of the transient cross-links in dictating diffusive behavior on length scales beyond the radius of gyration [11,30].

In addition to self-diffusion, cooperative diffusion in polymer gels is a long-standing topic of interest due to the coupling between network elasticity and dynamic fluctuations

*bdolsen@mit.edu

caused by long-range connectivity [31–36]. In contrast to self-diffusion, which involves the center-of-mass motion of individual chains through the gel, cooperative diffusion describes the collective fluctuations of the network-forming chains without regard to the displacement of any individual molecule [37,38]. As such, cooperative diffusion is commonly observed in quasielastic light and neutron scattering measurements in the absence of specifically labeled chains [39,40]. In a semidilute solution, these fluctuations are believed to pertain to the relaxation of polymer segments on the order of the blob size ξ , giving rise to a diffusive timescale $\tau = 1/q^2 D_{\text{coop}}$, where q is the wave vector and D_{coop} is the cooperative diffusion coefficient (distinct from the self-diffusion coefficient) [37]. Because the driving force for cooperative diffusion is the solution's osmotic modulus, D_{coop} is predicted to *increase* with volume fraction ϕ due to the increase in the restoring force to dissipate fluctuations, with $D_{\text{coop}} \sim \phi^{0.75}$ predicted in a good solvent [37,38].

In a polymer gel containing transient or permanent cross-links, elasticity from the junctions is believed to further suppress dynamic fluctuations such that cooperative diffusion (also called the gel mode) is *faster* than that of the analogous semidilute solution by a factor proportional to the elastic modulus [34,41,42]. However, in contrast to the predictions for semidilute solutions which have been largely well validated [39,43], the role of the cross-links in governing segmental and collective dynamics in gels remains controversial. Classical theories often assume that the osmotic modulus and segmental friction in the gel are equal to those of the analogous solution and unaffected by cross-linking, which are strong assumptions often not satisfied in experimental systems [44]. Thus, it remains difficult to predict the effects of important parameters underlying polymer network design, including the cross-link density, strand length, and chain architecture, on cooperative diffusion in gels [31,41]. This is evidenced by the broad range of cooperative diffusion behavior seen in gels experimentally: While some studies show an increase in D_{coop} with cross-link density consistent with the increase in elastic modulus [10,31,44–47], others observe a slowing of local dynamics attributed to chain tethering by the cross-links [32,36,48–50]. It is also unclear to what extent static structural features in the gel, such as the distance between elastically active cross-links, govern segmental dynamics, including on smaller length scales where a transition to single-chain behavior is sometimes observed [32,36,51]. Recent simulations have predicted a critical role of the interjunction spacing in defining a length scale for molecular caging, with chain diffusion unable to occur over larger length scales in the absence of junction exchange [11,30].

This work presents a fundamental study on the effect of associative binding on segmental dynamics in associative polymer gels, using neutron spin-echo (NSE) spectroscopy to probe the effects of important network parameters such as the cross-link density, strand length, and polymer architecture on dynamics close to the molecular radius of gyration. The model associative gels are formed by artificial coiled-coil proteins with a well-defined junction functionality and perfect monodispersity, thus forming an ideal system for studies of gel dynamics [22,25,52,53]. The NSE results illustrate changes in segmental dynamics with variations in strand

length, concentration, and sticker distribution (telechelic vs spaced along the backbone). A slowing of cooperative diffusion with increasing junction density is observed, hypothesized to occur due to an increase in the local viscosity due to the junctions that hinders segmental motion. Notably, the relaxation rates for all gels are found to collapse onto a master curve when scaled by the static junction spacing identified by small-angle neutron scattering, suggestive of self-similar dynamics in networks with different strand lengths and chain architectures. Finally, on long timescales (but shorter than the junction exchange time) a suppression of relaxation is observed, which is attributed to a freezing of chain dynamics due to binding and is estimated to occur on length scales close to the correlation length of the overlapping strands.

II. EXPERIMENTAL METHODS

Protein hydrogel synthesis. Deuterated water (99.9% deuterated) was purchased from Cambridge Isotope Laboratories. All other materials were purchased from Sigma-Aldrich or VWR. All materials were used as received. The model associative proteins PC₁₀P, PC₃₀P, and C₁₀(PC₁₀)₄ are formed by a multiblock architecture consisting of coiled-coil domains (“P”) separated by flexible midblocks (“C_x”), as shown in Fig. 1. Their encoding genes, amino acid sequences, and synthetic protocols have been previously reported [53,54]. Genes were engineered in the pQE9 vector, which confers ampicillin resistance, and transformed into the SG13009 cell line of *Escherichia coli*, which contains the pREP4 plasmid that confers additional kanamycin resistance. Transformed cells were grown on LB-agar plates at 37 °C overnight and used to seed 50 ml LB starter cultures. Saturated starter cultures were used to seed 5 l of TB media supplemented with 200 mg/l ampicillin and 50 mg/l kanamycin for antibiotic selection. Cells were grown at 37 °C until reaching an optical density of 0.8–1.0 at 600 nm and then induced with 1 mM isopropyl β -D-1-thiogalactopyranoside (IPTG). Protein expression proceeded for 6 h, after which cells were harvested by centrifugation and resuspended in denaturing buffer (8 M urea, 100 mM sodium phosphate, 10 mM tris, pH = 8.0). Cells were lysed by sonication, clarified by centrifugation, and purified by Ni²⁺-affinity chromatography, ammonium sulfate precipitation, and anion exchange chromatography in denaturing conditions. Purified proteins were dialyzed into Milli-Q water and lyophilized to yield a white cottonlike powder. Typical yields were 200 mg/l culture for PC₁₀P, 100 mg/l culture for PC₃₀P, and 100 mg/l culture for C₁₀(PC₁₀)₄. Protein purity was verified by sodium dodecyl sulfate polyacrylamide gel electrophoresis (SDS PAGE), as shown in Fig. S1 in the Supplemental Material [55] (also see [56–72]).

Associative network hydrogels were formed by dissolving lyophilized proteins in 100 mM sodium phosphate buffer at pH = 7.6 at the desired concentration. Concentrations were calculated assuming a protein density of 1.3 g/ml from previous work [22]. For neutron scattering experiments, gels were prepared in a deuterated buffer (100 mM sodium phosphate in D₂O, pH = 7.6) to enhance scattering contrast between polymer and solvent. Samples were stored at 4 °C for 2 days until they formed macroscopically homogeneous, optically clear hydrogels.

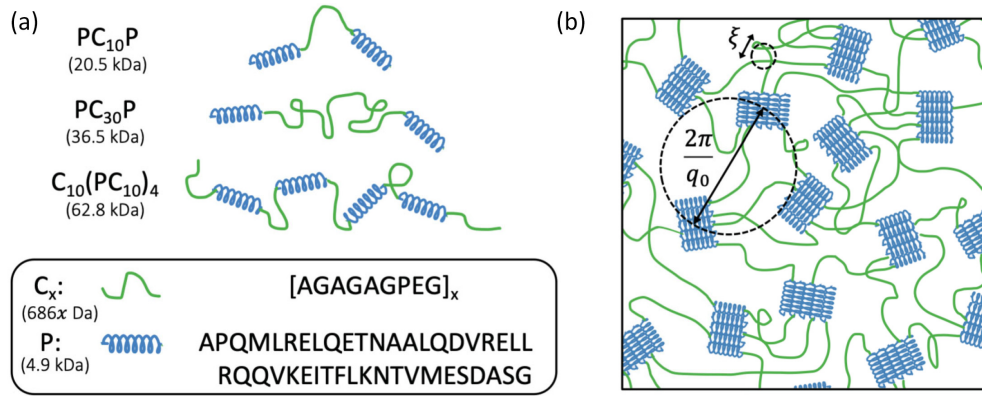


FIG. 1. (a) Schematics of the three artificial coiled-coil proteins used as model associative network hydrogels in this work along with the amino acid sequences of each domain. The molar mass of each C repeat is 686 Da and the molar mass of the P block is 4.9 kDa. (b) Schematic of the associative network formed by coiled-coil association in pentameric bundles. The interjunction domain size estimated from $2\pi/q_0$ and the local correlation blob length ξ (both obtained from small-angle neutron scattering) are indicated as static length scales.

Small-angle neutron scattering. Small-angle neutron scattering (SANS) measurements were performed on the EQ-SANS beamline at the Spallation Neutron Source at Oak Ridge National Laboratory. Two instrument configurations were used to cover a q range of $0.5\text{--}7.3\text{ nm}^{-1}$. The low- q configuration had a sample-to-detector distance of 4 m and a wavelength of 10 \AA , while the high- q configuration had a sample-to-detector distance of 2.5 m and a wavelength of 2.5 \AA . The EQ-SANS instrument uses a $1\times 1\text{ m}^2$ ^3He -tube detector with a resolution of $5.5\times 4.3\text{ mm}$ to detect scattered neutrons. All data were collected using a 10 mm beam aperture size.

Protein gels were sandwiched between two quartz windows with a 1 mm Ti spacer and sealed in a Ti demountable cell. Sealed samples were then annealed at 80°C for 5 min to remove thermal history and allow bubbles to float to the top of the cell outside of the 10 mm beam aperture. Measurements were performed at 25°C and 35°C . Samples were allowed to equilibrate at the SANS measurement temperature for 30 min before acquiring data. Scattered intensities were azimuthally averaged to convert them into one-dimensional (1D) scattering patterns, corrected for empty cell scattering and blocked beam background, and calibrated to an absolute scale using a Porasil silica standard. The data from the two configurations were stitched together after 1D data reduction by matching overlapping q ranges using DRTSANS software [73]. Solvent background subtraction was also performed by using a protein volume fraction calculated assuming a protein density of 1.3 g/ml [22].

Neutron spin-echo spectroscopy. Neutron spin-echo (NSE) spectroscopy was performed on the NSE beamline at the Spallation Neutron Source at Oak Ridge National Laboratory. Gel samples were spread onto aluminum front-loading cells with a path length of 1 mm and sealed with indium wire. Sealed samples were then annealed at 80°C for 5 min to remove thermal history and equilibrated at the NSE measurement temperature of 35°C for 30 min prior to data acquisition. Samples were aligned using a neutron camera and the scattering window was reduced to $3\text{ cm}\times 3\text{ cm}$. Two instrument wavelengths (8 and 11 \AA) were used to capture a q range of $0.32\text{--}1.8\text{ nm}^{-1}$ and a Fourier time range of $0.1\text{--}130\text{ ns}$. Instrument resolution

was measured using Grafoil stacked graphite sheets (mid- and high- q) and aluminum oxide (low- q).

In the NSE technique, the velocity of each scattered neutron is encoded into its individual phase angle as it undergoes symmetric Larmor precessions before and after scattering off the sample, which decouples the detectability of velocity changes from the monochromaticity of the incident beam [40]. The spin-echo amplitude is proportional to the normalized coherent intermediate scattering function at the time equal to the Fourier time τ :

$$\tau = \frac{\gamma_N J m_N^2}{2\pi h^2} \lambda^3, \quad (1)$$

where γ_N is the neutron's gyromagnetic ratio, $J = \int B \cdot dl$ is the magnetic field integral along the longitudinal axis of each precession coil, h is Planck's constant, and λ is the neutron wavelength. Data at each position of the detector were reduced to get the normalized intermediate scattering function $I(q, t)/I(q, 0)$ with solvent background correction:

$$\frac{I(q, t)}{I(q, 0)} = \left[\frac{2(A_P - T A_b)}{(U - D)_P - T(1 - \phi_P)(U - D)_b} \right] / \left(\frac{2A}{U - D} \right)_{\text{res}}. \quad (2)$$

Here, A_i is the amplitude of the spin echo of species i , T is the ratio of transmissions of the sample to the background, U is the number of counts with no spin flip ("spin up," $\pi/2$, and π flippers off), and D is the number of counts with a spin flip ("spin down," $\pi/2$ flippers off, π flipper on). In Eq. (2), there are three types of scatterers (species i): Protein (P), solvent background (b), and resolution (res). Once $I(q, \tau)$ was obtained at each detector position, the data were binned and combined based on a set of 15 q arcs corresponding to different zones on the detector.

Linear rheology. Oscillatory shear rheology was performed on an Anton Paar MCR 301 rheometer using a cone and plate geometry (25 mm , 1°). Mineral oil was used to coat the sides of the geometry to prevent dehydration during measurement. Gels were held at 45°C for 30 min to allow them to relax and equilibrated at the measurement temperature for 30 min before acquiring data. Storage and loss moduli were obtained

over a frequency range of 0.01–100 rad/s using a strain of 2%, which is within the linear viscoelastic regime [22,53]. All measurements were performed at 35 °C.

Pulsed field gradient nuclear magnetic resonance spectroscopy. Pulse field gradient nuclear magnetic resonance (PFG NMR) was performed on a 400 MHz Bruker Avance-III HD Nanobay spectrometer equipped with a 5 mm liquid-nitrogen cooled Prodigy broadband cryoprobe and a SampleXpress 60 autosampler. Protein gels were loaded via centrifugation into 5 mm NMR tubes at 70 °C and annealed at 37 °C overnight to allow for relaxation. Samples were thermally equilibrated for 30 min prior to spectral acquisition at 25 °C. One-dimensional ¹H NMR spectra were collected at 25 °C while spinning at 20 rpm via a longitudinal eddy current delay bipolar gradient pulse with a gradient pulse duration and diffusion delay of 2 and 50 ms, respectively.

III. RESULTS AND DISCUSSION

Model associative network formed by artificial coiled-coil proteins. The artificial coiled-coil proteins PC₁₀P, PC₃₀P, and C₁₀(PC₁₀)₄ form unentangled viscoelastic hydrogels above the overlap concentration (~5% w/v) in aqueous buffer. Each protein has a multiblock architecture consisting of α -helical domains (“P”) connected by flexible linkers (“C_x,” with $x = 10, 30$), resulting in total molar masses of 20.5 kDa for PC₁₀P, 36.5 kDa for PC₃₀P, and 62.8 kDa for C₁₀(PC₁₀)₄. Structures of the three proteins and amino acid sequences of the P and C_x domains are provided in Fig. 1. The P domains associate into pentameric rodlike bundles with dimensions of 3.0 nm diameter and 7.3 nm length, serving as physical cross-links to form a space-spanning gel [25,74]. The C_x domains behave as random coils in solution [52], serving as elastic strands that bridge the junctions. Because of their sequence-defined chain architecture, well-defined association chemistry, and perfect monodispersity, the coiled-coil proteins are expected to form an ideal model system for studying associative network dynamics [22,53], without sources of molecular heterogeneity such as irregular strand length and sticker distribution, which are typically found in polymer gels.

Shear rheology and small-angle neutron scattering (SANS) characterization of the protein gels demonstrate viscoelastic and structural features typical of transient networks. Frequency sweeps reveal a high-frequency plateau modulus and a crossover between storage and loss moduli indicating macroscopic relaxation (Fig. S10 [55]). The exchange time of the coiled-coil junctions can be estimated [22,75] from the crossover frequency of the storage and loss moduli via $\tau_{ex} \approx 1/\omega_c$, ranging from 0.1 to 50 s at 35°. Note that while the junction exchange times are expected to be correlated to the crossover frequency, they may not be quantitatively equal [76]. The crossover frequencies show a strong dependence on the chain architecture (telechelic vs midblock functionalized), with the C₁₀(PC₁₀)₄ crossover frequency being ~100-fold larger than those for PC_xP (see Table S3 in the Supplemental Material [55] for estimated values of τ_{ex}). This difference in the crossover frequencies between C₁₀(PC₁₀)₄ and PC_xP may be related to steric effects of the C_x strands surrounding the coiled-coil domains, with C₁₀(PC₁₀)₄ containing two strands flanking each P domain but PC_xP containing only one.

However, the exchange times of all protein gels are several orders of magnitude longer than the timescales accessed by NSE (~1–100 ns), allowing each gel to be approximated as a topologically permanent network during the measurement timescale.

SANS characterization (Fig. S2 [55]) reveals at least two structural length scales in the associative protein gels, which can be quantified by fitting the scattering patterns to a semiempirical correlation length model (see the Supplemental Material for details [55]). These length scales comprise (1) a static domain size $d \approx 10$ –30 nm attributed to the average distance between coiled-coil junctions and (2) a smaller correlation length $\xi \approx 2$ –10 nm reflecting the blob size of the overlapping strands as in a semidilute solution [60]. Note that the interjunction spacing d can be clearly identified from the broad peak component of the scattering patterns due to the relatively large size of the assembled coiled-coil junctions [61,62]. This distinguishes the gels here from conventional polymer gels where a scattering feature is typically not seen at the interjunction spacing without labeling [44,51,60,63–65]. The interjunction spacings decrease with junction density roughly consistent with the expected scaling of $d \sim \rho_{\text{junction}}^{-1/3}$ (Fig. S3 and Table S1 [55]). However, across all gels spanning an order-of-magnitude range in junction density (see Fig. S3 [55]) the values of d are ~50% larger than both the theoretical spacing assuming randomly dispersed junctions (Supplemental Material [55]) and the estimated root-mean-square unperturbed end-to-end distance of a free C₁₀ or C₃₀ domain ($R_{C_{10}} = 6.6 \pm 0.7$ nm and $R_{C_{30}} = 13 \pm 1$ nm, assuming good-solvent conditions [66]), which may reflect chain stretching due to gelation or the presence of unattached stickers at equilibrium. Further details of the findings from SANS are provided in the Supplemental Material [55].

Effect of network architecture on segmental dynamics. Neutron spin-echo (NSE) measurements of the associative protein gels illustrate clear differences in segmental relaxation behavior caused by the underlying network architecture, including variations in the strand length, chain concentration, and number of stickers per chain. The q range of the NSE instrument of 0.32–1.80 nm⁻¹ corresponds to a real-space range of 3.5–20 nm, which is comparable to the length scales corresponding to the interjunction spacing ($2\pi/q_0$), molecular end-to-end distance of the C_x strands (R_{ee}), and segmental blob size (ξ), as shown in Table I. Within the accessible q range of the NSE measurements the neutron scattering signal is predominantly coherent (see Fig. S2 [55]), and the spin-echo intensity is proportional to the normalized coherent intermediate scattering function, $I(q, t)/I(q, 0)$, where

$$I(q, t) = \frac{1}{N} \sum_{i,j=1}^N \langle \exp(-iq \cdot [\mathbf{r}_i(t) - \mathbf{r}_j(0)]) \rangle, \quad (3)$$

with $\mathbf{r}_i(t)$ being the position of scattering center i at time t . For NSE measurements, gels were prepared by dissolving hydrogenated protein chains in a deuterated buffer to access the dynamic pair correlation function of the polymer segments in the gel, including both the coiled-coil and linker domains.

Dynamic scattering curves for each gel exhibit wave-vector-dependent decay profiles on timescales of

TABLE I. Structural length scales of the associative protein gels studied by NSE obtained from SANS measurements at 35 °C (data are provided at 35 °C to match NSE measurements) fit to the broad-peak model (Eq. (S1) [55]).

Protein	R_{ee} (nm) ^a	Concentration ^b (w/v)	Junction density $\times 10^3$ (nm ⁻³)	q_0 (nm ⁻¹)	$d = 2\pi/q_0$ (nm)	ξ (nm)
PC ₁₀ P	12 \pm 1	7% 12.5%	0.77 1.32	0.37 \pm 0.02 0.41 \pm 0.01	17 \pm 1 15 \pm 1	2.6 \pm 0.1 2.6 \pm 0.1
PC ₃₀ P	16 \pm 2	7% 12.5%	0.43 0.75	0.34 \pm 0.02 0.37 \pm 0.01	19 \pm 1 17 \pm 1	3.3 \pm 0.1 3.0 \pm 0.1
C ₁₀ (PC ₁₀) ₄	22 \pm 3	6.5%	0.48	0.35 \pm 0.01	17 \pm 1	2.7 \pm 0.1

^aEstimated from $R_{C_{10}} = 6.6 \pm 0.7$ nm and a good-solvent scaling $R_{ee} \sim M^{0.588}$.

^bConcentrations listed are those studied by NSE. Gel concentrations for each protein were chosen to approximately match the coiled-coil junction concentration across the different proteins, such that the effects of varying the C_x midblock length and chain architecture could be isolated.

~ 10 – 100 ns, as shown representatively for each protein in Figs. 2(a)–2(c). Scattering curves were first analyzed by calculating the initial decay rate, or first cumulant, defined as

$$\Gamma_0(q) = -\lim_{t \rightarrow 0} \frac{d}{dt} \ln \left[\frac{I(q, t)}{I(q, 0)} \right]. \quad (4)$$

The first cumulant analysis has the advantage of providing insight into the qualitative types of motion from the scaling of Γ_0 with q without requiring any assumptions about the exact form of the coherent scattering function for the network. For all gels, the dynamic scattering curves exhibit an initially

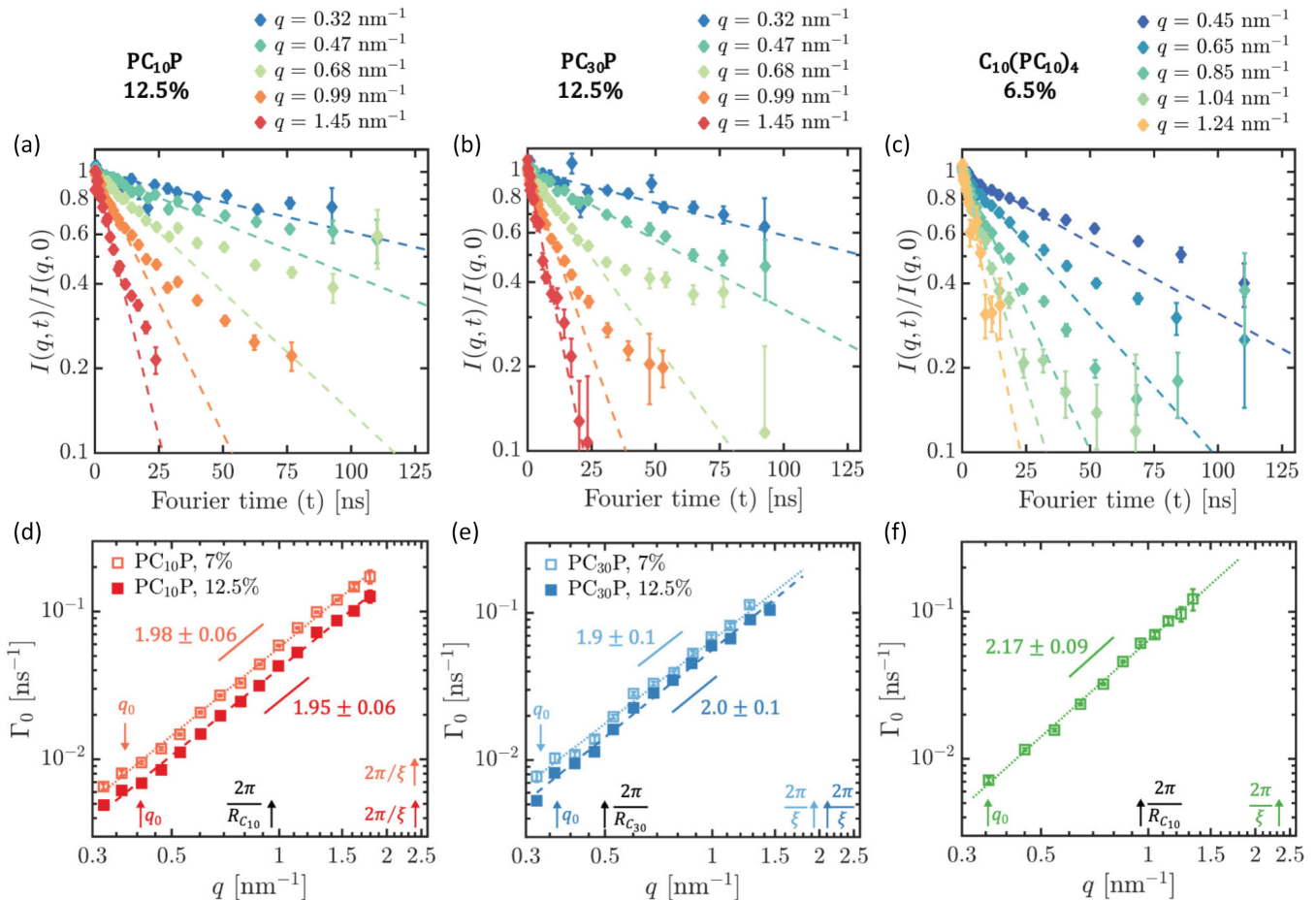


FIG. 2. Top: Representative dynamic coherent scattering curves at various wave vectors measured by neutron spin-echo spectroscopy for (a) PC₁₀P, 12.5% w/v; (b) PC₃₀P, 12.5% w/v; and (c) C₁₀(PC₁₀)₄, 6.5% w/v in deuterated buffer at 35 °C. Dashed lines are fits to the initial linear regime (on the semilogarithmic scale) to identify the first cumulant. Bottom: Scaling of the first cumulant with wave vector for (d) PC₁₀P (7% and 12.5% w/v), (e) PC₃₀P (7% and 12.5% w/v), and (f) C₁₀(PC₁₀)₄ (6.5% w/v). Error bars are standard deviations of first cumulant fits to 100 bootstrapped replicas of $I(q, t)/I(q, 0)$. Lines are power-law fits for each gel with scaling exponents and their 95% confidence intervals indicated. Arrows indicate length scales corresponding to the correlation peak wave vector q_0 from SANS, unperturbed root-mean-square end-to-end distance of the C_x strands, and correlation blob length ξ (see Table I).

linear decay when plotted on a semilogarithmic scale, validating the use of Eq. (4) to calculate the first cumulant at each wave vector.

The wave-vector dependence of the first cumulant for each protein is shown in Figs. 2(d)–2(f), where a single power-law regime is seen for all gels with an exponent consistent with diffusive scaling, i.e., $\Gamma_0 \sim q^2$. It is noteworthy that the initial decay rates for all gels follow diffusive scaling across the entire q range, displaying no transitions even at length scales corresponding to the geometric mesh size, root-mean-square end-to-end C_x strand distance, or interjunction spacing $2\pi/q_0$. This contrasts with previous NSE results on related protein and polymer gels, where a transition from diffusive scaling ($\Gamma_0 \sim q^2$) to Zimm-like scaling ($\Gamma_0 \sim q^3$) has been seen above a critical wave vector usually close to the inverse of a characteristic network mesh size, which is often assumed to be either the interjunction spacing or the correlation blob size [7,32,36,51]. In these studies, the low- q diffusive regime is typically attributed to cooperative diffusion (i.e., the gel mode [34]), while the high- q Zimm-like regime is typically attributed to internal single-chain modes roughly analogous to those of a free polymer in solution [38]. The purely diffusive scaling seen here is consistent with cooperative diffusion as seen previously on length scales above the mesh size. This is further validated by examining the dependence of Γ_0 vs q^2 on linear axes (Fig. S5 [55]), where a linear relationship with zero intercept is seen for all gels consistent with diffusive behavior. The results here suggest that cooperative diffusion is the dominant relaxation mode in the protein gels even down to the smallest accessible length scales probed, which approach the static correlation blob size ξ estimated from SANS. It is possible that this correlation blob size ξ (as opposed to the interjunction spacing $2\pi/q_0$) is the relevant length scale for the transition to single-chain behavior, which would be analogous to a semidilute solution [38]. It should be noted that the transition length scale may be altered by the chain conformational statistics of the proteins (e.g., stretching) due to associative binding, which has recently been reported in covalent polymer gels of similar concentrations [77]. However, this transition to Zimm-like behavior has yet to be confirmed experimentally in the associative protein gels here, and it is still unclear which length scale might govern the transition (if any) to single-chain behavior.

For all gels, apparent cooperative diffusion coefficients can be calculated from the wave-vector-normalized values of the first cumulants of the NSE curves via

$$D_{\text{coop}} = \frac{\Gamma_0}{q^2}. \quad (5)$$

In semidilute solutions, D_{coop} is predicted [38] to inversely depend on both the solvent viscosity η_s and the hydrodynamic correlation length ξ_h , which is on the order of the static correlation blob size [37], by the Stokes-Einstein law:

$$D_{\text{coop}} = \frac{k_B T}{6\pi \eta_s \xi_h}. \quad (6)$$

Though the validity of Eq. (6) for cross-linked gels is still under investigation [41], it has been widely employed to estimate hydrodynamic correlation lengths in both covalent and

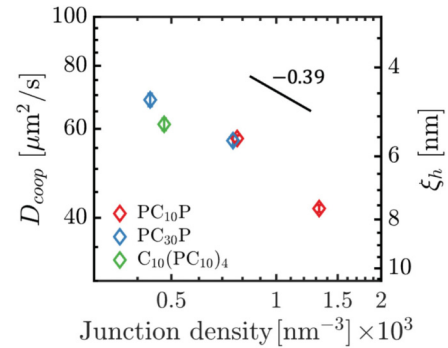


FIG. 3. Apparent cooperative diffusion coefficients calculated using Eq. (5) vs total junction density from NSE measurements at 35 °C, along with apparent hydrodynamic correlation lengths calculated using Eq. (6) assuming an unperturbed solvent viscosity of $\eta_s = 0.71$ mPa s. Apparent diffusion coefficients are averaged over all wave vectors. Error bars represent standard errors and are smaller than the markers.

associative polymer gels, with the assumption that the local dynamics is analogous to that of an un-cross-linked solution at the same concentration [10,31,70].

Apparent cooperative diffusion coefficients calculated from the NSE data using Eq. (5) are examined as a function of total coiled-coil junction concentration in Fig. 3. The diffusion coefficients are on the order of cooperative diffusion coefficients seen in covalently cross-linked polymer gels [31,44,78], suggesting similarities in their local structure and dynamic timescales. Importantly, the diffusion coefficients for the different proteins appear to decrease with both total protein weight fraction (when comparing gels of the same protein) and total junction density (across all proteins). This suggests a potentially important role of the junctions in governing cooperative diffusion in protein gels, even across differences in the length and number of C_x midblocks per chain. The concentration dependences of D_{coop} seen here are in contrast to the classical predictions for both gels and solutions [34,37], which predict an increase in the cooperative diffusivity with concentration and junction density due to the enhancement in the restoring force for dissipating fluctuations [34]. Note the macroscopic elastic modulus of the protein gels increases with concentration, as expected (Table S3 [55]). However, the enhanced elasticity does not appear to increase the rate of cooperative diffusion in these gels.

From the cooperative diffusion coefficients, Eq. (6) can be used to estimate *apparent* hydrodynamic correlation lengths ξ_h in the protein gels as shown in the right-hand ordinate of Fig. 3, where the unperturbed viscosity of $\eta_s = 0.71$ mPa s at 35 °C was used in the estimates of ξ_h . The apparent hydrodynamic correlation lengths here are of the same order of magnitude as the static correlation lengths ξ and ξ_{OZ} obtained from SANS (Table S1 [55]), as well as hydrodynamic correlation lengths previously measured in other cross-linked polymer gels by dynamic light scattering [10,31,36,70]. Quantitatively, the values of ξ_h are \sim twofold larger than the values of the static length scales ξ and ξ_{OZ} , though it should be noted that the calculated values of ξ_h may be inaccurate due to the use of the unperturbed solvent

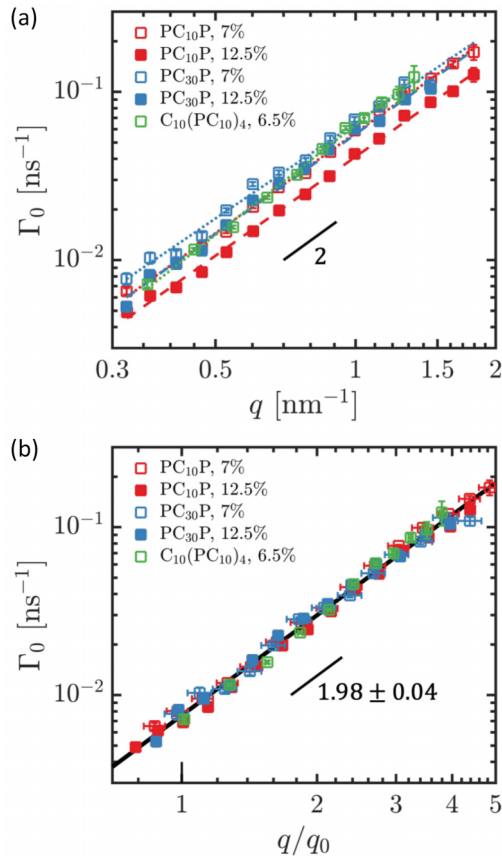


FIG. 4. (a) Comparison of the initial decay rates as a function of wave vector for all the protein gels. (b) Master curve of initial decay rates as a function of dimensionless wave vector, demonstrating a combined scaling of $\Gamma_0 \sim (q/q_0)^{1.98 \pm 0.04}$.

viscosity in their estimation. Because of the concentration dependence of D_{coop} , the calculated hydrodynamic correlation lengths *increase* with junction density and concentration, in contrast to theoretical predictions and previous experimental findings in synthetic polymer gels [10,31,37].

The concentration dependence of cooperative diffusion in the protein gels is further exemplified by a comparison of their wave-vector-dependent decay rates [Fig. 4(a)], where all gels exhibit the same behavior in their decay rates to within a shift factor. The wave vector can be rescaled by the correlation peak wave vector q_0 observed by SANS, which is attributed to the average distance between cross-links (i.e., the elastic mesh size) as discussed earlier. As shown in Fig. 4(b), the relaxation rates for all gels appear to collapse onto a master curve when plotted against the dimensionless wave vector q/q_0 , with a combined scaling of $\Gamma_0 \sim (q/q_0)^{1.98 \pm 0.04}$. This suggests a renormalizing effect of the correlation peak q_0 on gel dynamics, where it defines a characteristic length scale governing self-similar relaxation behavior between different networks. In particular, the increase of q_0 (or equivalently, the decrease in interjunction spacing) with junction density may manifest as a reduction in the effective length scale of segmental dynamics in the gel, suggesting an important role of the interjunction spacing in dictating cooperative diffusion even across differences in strand length and chain architecture.

The importance of the interjunction spacing in governing dynamics in cross-linked gels has been previously suggested by mesoscale hydrodynamic simulations of internal dynamics in microgels consisting of end-linked chains connected by tetrafunctional junctions [79,80]. In these simulations, a crossover from Zimm relaxation to cooperative diffusion is seen at a critical wave vector of $q = 2\pi/R_{ee}$, where R_{ee} is the root-mean-square end-to-end length of the strands between stickers, which defines the junction spacing. In addition, the segmental decay rates for networks with different strand lengths fall onto a master curve when plotting $\Gamma\tau_Z$ vs qR_{ee} , where $\tau_Z \sim N^{3\nu}$ is the Zimm relaxation time for a single strand (with N being the strand degree of polymerization and ν being the Flory exponent). These simulations suggest a self-similar nature of segmental dynamics in cross-linked gels, similar to the NSE results here, where the average distance and relaxation time of the strands between junctions provide the characteristic length and timescales governing their dynamics. However, a key difference between the simulation and experimental results is the role of the strand Zimm time in defining the relaxation timescale in the gel to collapse the curves, instead requiring only rescaling of the length dimension. This suggests that the gel dynamics observed by NSE may depend only weakly on the relaxation of the strands, the rate of which should vary between the C₁₀ and C₃₀ midblocks via $\tau_Z \sim N^{1.8}$ in a good solvent [38]. This is most clearly illustrated by comparing the data for the PC₁₀P 7% and PC₃₀P 12.5% gels in Fig. 4(a) and Fig. S3 [55]; these gels have nearly identical junction densities and correlation peak wave vectors and quantitatively equal relaxation rates, despite the \sim sevenfold longer Zimm time of the C₃₀ strands compared to C₁₀.

Collectively, the NSE data suggest the presence of additional factors that suppress segmental dynamics in the associative protein gels, resulting in a slowing of cooperative diffusion with junction density contrary to scaling predictions. It is hypothesized that the suppression of cooperative diffusion may arise from crowding effects from the overlapping chains and pentameric junctions, which may enhance the local viscosity beyond that of the solvent alone [81]. The artificial proteins are connected by rodlike α -helical junctions, the presence of which may increase the local viscosity through hydrodynamic and excluded volume effects [81,82]. Similar effects have also been seen in covalently cross-linked polymer gels, where enhancements in the effective local viscosity by as much as sevenfold have been reported from relaxation rates in the high- q Zimm-like regime [7,31,83]. To directly test the effect of chain concentration on the local friction in the gel, self-diffusion measurements of the water solvent in the protein hydrogels were performed using pulsed field gradient nuclear magnetic resonance spectroscopy (see the Supplemental Material for full details [55]). These measurements reveal a slowing of the water self-diffusivity with increasing protein concentration, suggesting an enhancement in the local friction due to the associative proteins consistent with the observed slowing of cooperative diffusion of the proteins with concentration. It should be noted that other studies of synthetic polymer gels have observed no increase in effective viscosity

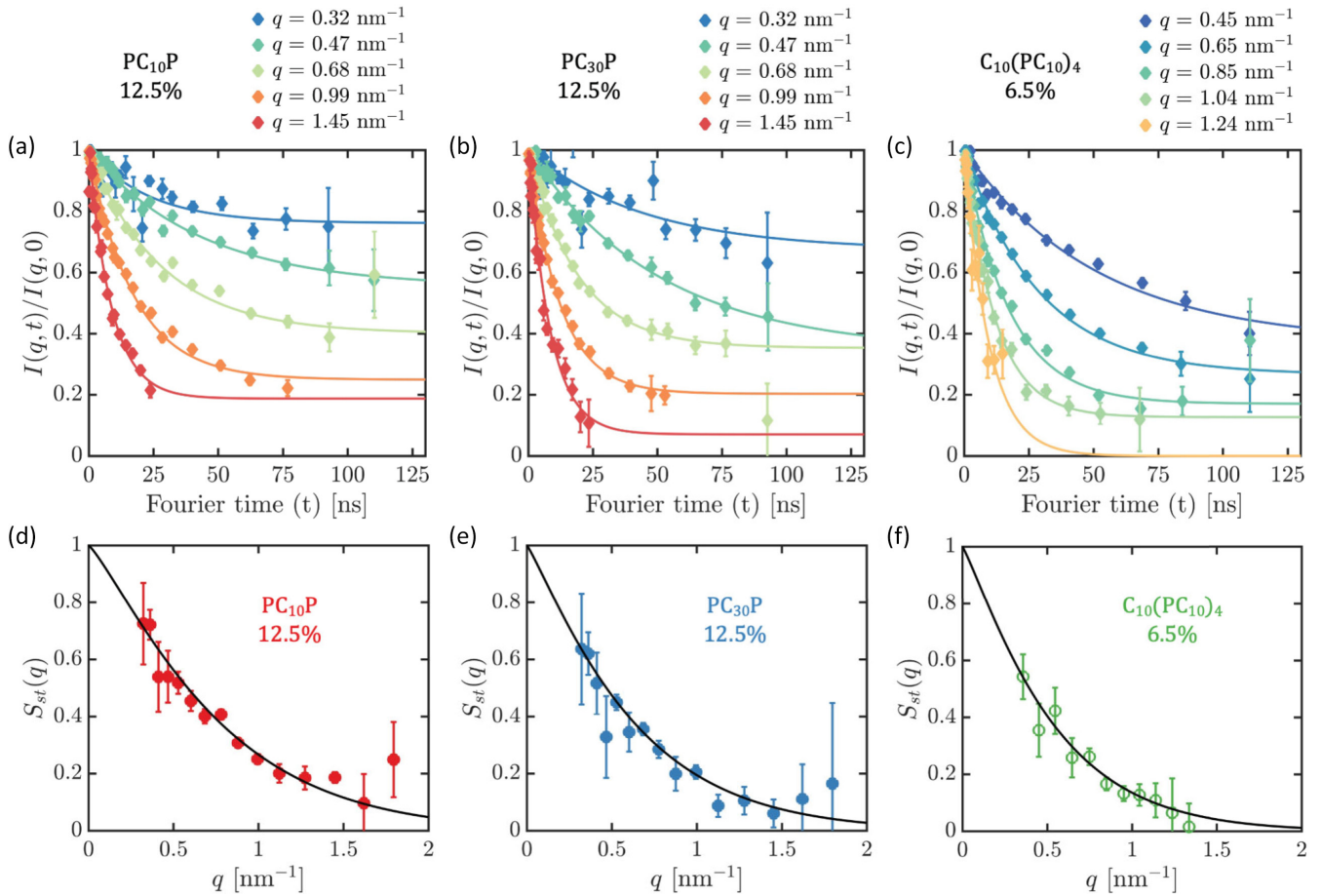


FIG. 5. (a)–(c) Representative fits to Eq. (8) of the dynamic scattering curves for each protein gel at 35 °C. (d)–(f) Fractional static component of the intermediate scattering function for each gel. Error bars are standard deviations of 100 bootstrapped replicas of $I(q, t)/I(q, 0)$ each fit to Eq. (8). Lines are fits to the modified Guinier function [Eq. (9)] using weighted nonlinear least squares.

compared to the solvent alone, even at comparable concentrations [10,31], suggesting a complex interplay between chain and solvent dynamics in the protein gels that govern local relaxation.

While the first cumulant analysis captures the initial (logarithmic) slope of the dynamic scattering curves for the associative protein gels, the curves deviate from the purely exponential decay predicted by the linear fit, instead appearing to plateau at a finite value above timescales ~ 50 – 100 ns (note that these timescales are still significantly shorter than the gels' rheological relaxation time of ~ 1 – 10 s). This plateau may be related to the confinement of chain motion to a certain length scale due to tethering from the junctions, causing a nondecaying elastic component to the intermediate scattering function; analogous effects have been seen in cross-link and strand motion in covalent polymer networks [32,44,51,84]. Similar to previous studies [32,51], the nondecaying component in the NSE curves can be quantified by decomposing the intermediate scattering function into a sum of an inelastic, time-dependent component, $S_{\text{dyn}}(q, t)$, and an elastic, time-independent component, $S_{\text{st}}(q)$:

$$\frac{I(q, t)}{I(q, 0)} = [1 - S_{\text{st}}(q)]S_{\text{dyn}}(q, t) + S_{\text{st}}(q), \quad (7)$$

where $S_{\text{dyn}}(q, t)$ and $S_{\text{st}}(q)$ are normalized dynamic and static scattering components, respectively. From the diffusive scaling seen in all gels, $S_{\text{dyn}}(q, t)$ is assumed to follow a single-exponential decay with time constant approximately equal to the inverse decay rate; this is identical to functional forms used in previous studies [32,51]:

$$\frac{I(q, t)}{I(q, 0)} = [1 - S_{\text{st}}(q)] \exp\left(-\frac{t}{\tau}\right) + S_{\text{st}}(q). \quad (8)$$

Equation (8) provides reasonable fits to the NSE dynamic scattering curves as shown in Figs. 5(a)–5(c), where the fractional static component $S_{\text{st}}(q)$ is seen as the long-time plateau in the relaxation function. Deviations in the fits may arise from the presence of a broad spectrum of relaxation modes or a well-separated second mode with a longer time constant. However, because any additional relaxation modes are not fully developed within the accessible Fourier time window, approximating $S_{\text{dyn}}(q, t)$ by an empirical stretched exponential or sum of two exponentials with different time constants results in noisy fits with large uncertainties in the fit parameters (Supplemental Material [55]). Thus, Eq. (8) is used for further analysis due to its simplicity and ability to capture the nondecaying component of the NSE curves with reasonable accuracy and a minimal number of parameters.

For each protein, the amplitude of the nondecaying component $S_{st}(q)$ is observed to decrease with increasing wave vector [Figs. 5(d)–5(f)], consistent with an increase in segmental mobility on smaller length scales as expected. Fitting the static component $S_{st}(q)$ with a phenomenological modified Guinier function [51,84] allows a characteristic length scale governing the extent of dynamic fluctuations in the gel to be estimated,

$$S_{st}(q) = \exp \left[- \left(\frac{\Xi_{\text{fluc}}^2 q^2}{3} \right)^\beta \right], \quad (9)$$

where Ξ_{fluc} is a fluctuation length scale and β is a stretching parameter ranging from 0 to 1 reflecting the spectrum of fluctuation length scales. The case of $\beta = 1$ corresponds to a Gaussian fluctuation distribution for which the classical Guinier function is recovered, whereas $\beta < 1$ corresponds to a broader-than-Gaussian distribution.

The decrease in the $S_{st}(q)$ with q can be reasonably captured by Eq. (9) [Figs. 5(d)–5(f)], with the best-fit fluctuation length scales Ξ_{fluc} ranging from 2.1 to 3.5 nm for all gels. It should be noted that because the NSE scattering curves reflect coherent (i.e., pairwise) dynamics of the polymers in the network, Ξ_{fluc} does not correspond directly to a root-mean-square segmental displacement (of either junctions or strands) [51,84]. Rather, Ξ_{fluc} can be regarded as a characteristic length scale above which the network is topologically frozen on the timescale of the NSE measurement, such that concentration fluctuations cannot be relaxed by segmental motion alone but instead require network rearrangement mediated by junction exchange [7]. The stretching parameter β from fits to Eq. (9) ranges between 0.5 and 0.8 (see Fig. S7 [55]), reflecting a distribution of fluctuation length scales. This heterogeneity may be related to variations in local network topology (e.g., the presence of loops) which can create nonuniformities in the junction elastic effectiveness and alter the extent of local chain confinement [85].

Brownian dynamics simulations have predicted a strong role of the interjunction spacing (i.e., the elastic mesh size) in governing caging behavior in associative polymer self-diffusion, resulting in a sharp increase in the diffusion timescale due to the need for at least one sticker to unbind and effect network rearrangement [11,30]. The dynamic fluctuation length scales, Ξ_{fluc} , calculated from fits to Eq. (9), are expected to be related to this caging transition by reflecting a maximal length scale for segmental diffusion at which point chain motion becomes restricted. In Fig. 6, the values of Ξ_{fluc} for all the protein gels are compared with other static and dynamic length scales in the gel, including the interjunction spacing $d = 2\pi/q_0$, root-mean-square end-to-end distances of the C_{10} and C_{30} strands, static correlation blob length ξ , and the hydrodynamic blob length ξ_h . The dynamic fluctuation length scales Ξ_{fluc} are ~ 5 times smaller than the interjunction spacing, significantly lower than predicted by simulation, and are instead close to the correlation blob length ξ . The discrepancies between Ξ_{fluc} and $2\pi/q_0$ may be due to additional hindrances to segmental motion beyond that of junction tethering alone that are not captured in the simulations or the contributions of interchain correlations to the NSE data compared to the single-chain dynamics probed by simulation

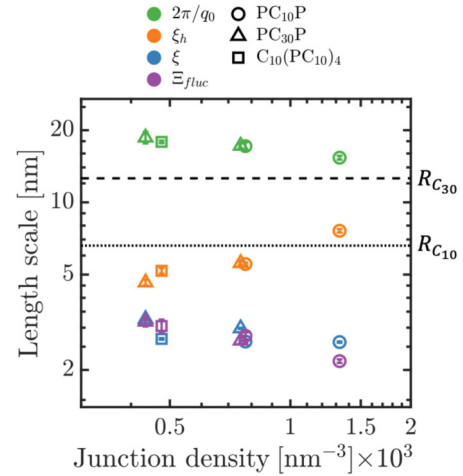


FIG. 6. Comparison of the dynamic fluctuation length scale Ξ_{fluc} , interjunction spacing $2\pi/q_0$, correlation blob length ξ , and apparent hydrodynamic correlation length ξ_h vs junction density for all protein gels. The root-mean-square end-to-end distance of the C_{10} and C_{30} strands are shown for comparison. All data measured at 35 °C.

[11,30]. It should be noted that all the protein gels are in the unentangled regime [22], such that topological hindrances to segmental motion should be minimal. Thus, further study is required to conclusively assign the factors governing the dynamic fluctuation length scale Ξ_{fluc} and its relationship to the other characteristic length scales in the gel. Interestingly, while most of the length scales shown in Fig. 6 appear to slightly decrease with junction density, consistent with a reduction in the characteristic network mesh size as expected [37], the hydrodynamic correlation length ξ_h [calculated from the cooperative diffusion coefficients using Eq. (6)] exhibits a clear increase with junction density. This further provides evidence for distinct origins for the dynamic and static behavior of the associative gels, again suggesting additional factors in the gel that suppress segmental dynamics without perturbing the static network structure.

IV. CONCLUSIONS

The combination of static and dynamic neutron scattering measurements on model associative protein gels indicates a complex role of transient binding on segmental fluctuations of the network-forming chains on length scales close to their radius of gyration, manifesting across systematic variations in the strand length, sticker density, and molecular architecture. All gels are found to exhibit a short-time diffusive mode on all wave vectors, attributed to cooperative diffusion of the overlapping chains, without sign of a transition at any known structural length scale in the gel. The cooperative diffusion rates decrease with total junction density, contrary to classical scaling predictions, suggesting additional factors that hinder segmental motion arising from the coiled-coil junctions. By rescaling the wave vector by a correlation peak wave vector attributed to the average distance between coiled-coil junctions, the relaxation rates of all gels collapse onto a master curve, indicating the importance of the interjunction spacing in renormalizing cooperative diffusion in networks with

different strand lengths and chain architectures. Finally, on long timescales a suppression of relaxation is observed on all gels, reflecting a freezing of chain dynamics due to tethering before the onset of junction exchange. From the amplitude of the nondecaying component in the spin-echo intensity, a characteristic length scale corresponding to the extent of dynamic fluctuations can be estimated, which is found to be smaller than the interjunction spacing but close to the correlation blob size. Collectively, these results demonstrate complex effects of underlying network parameters on segmental motion in associating polymer gels and may be generalizable to other transiently and permanently cross-linked gels with different sticker chemistry and chain architecture.

ACKNOWLEDGMENTS

This work was supported by the National Science Foundation under Award No. DMR-1709315 and the Department of Energy under Award No. DE-SC0007106. A.R. acknowledges support from the Department of Defense through a National Defense Science and Engineering Graduate Fellowship. The authors acknowledge Danielle J. Mai for assistance with protein synthesis, Piotr Zolnierczuk and Mary Odom for assistance with neutron spin-echo measurements, and Changwoo Do, Carrie Gao, and William Heller for assistance with small-angle neutron scattering measurements.

The authors declare no competing financial interest.

-
- [1] M. J. Webber, E. A. Appel, E. W. Meijer, and R. Langer, *Nat. Mater.* **15**, 13 (2015).
- [2] K. Liu, Y. Kang, Z. Wang, and X. Zhang, *Adv. Mater.* **25**, 5530 (2013).
- [3] S. Frey, R. P. Richter, and D. Görlich, *Science* **314**, 815 (2006).
- [4] Y. J. Yang, D. J. Mai, T. J. Dursch, and B. D. Olsen, *Biomacromolecules* **19**, 3905 (2018).
- [5] D. Y. Wu, S. Meure, and D. Solomon, *Prog. Polym. Sci.* **33**, 479 (2008).
- [6] O. R. Cromwell, J. Chung, and Z. Guan, *J. Am. Chem. Soc.* **137**, 6492 (2015).
- [7] A. Rao, H. Yao, and B. D. Olsen, *Phys. Rev. Res.* **2**, 043369 (2020).
- [8] S. Tang and B. D. Olsen, *Macromolecules* **49**, 9163 (2016).
- [9] S. Hackelbusch, T. Rossow, P. Van Assenbergh, and S. Seiffert, *Macromolecules* **46**, 6273 (2013).
- [10] T. Rossow, A. Habicht, and S. Seiffert, *Macromolecules* **47**, 6473 (2014).
- [11] A. Rao, J. Ramírez, and B. D. Olsen, *Macromolecules* **54**, 11212 (2021).
- [12] P. B. Rapp, A. K. Omar, J. J. Shen, M. E. Buck, Z. G. Wang, and D. A. Tirrell, *J. Am. Chem. Soc.* **139**, 3796 (2017).
- [13] P. B. Rapp, A. K. Omar, B. R. Silverman, Z.-G. Wang, and D. A. Tirrell, *J. Am. Chem. Soc.* **140**, 14185 (2018).
- [14] Q. Chen, G. J. Tudryn, and R. H. Colby, *J. Rheol. (NY, US)* **57**, 1441 (2013).
- [15] W. C. Yount, D. M. Loveless, and S. L. Craig, *J. Am. Chem. Soc.* **127**, 14488 (2005).
- [16] D. E. Fullenkamp, L. He, D. G. Barrett, W. R. Burghardt, and P. B. Messersmith, *Macromolecules* **46**, 1167 (2013).
- [17] F. Tanaka and S. F. Edwards, *Macromolecules* **25**, 1516 (1992).
- [18] A. Tripathi, K. C. Tam, and G. H. McKinley, *Macromolecules* **39**, 1981 (2006).
- [19] M. Rubinstein and A. N. Semenov, *Macromolecules* **31**, 1386 (1998).
- [20] R. S. Hoy and G. H. Fredrickson, *J. Chem. Phys.* **131**, 224902 (2009).
- [21] L. Leibler, M. Rubinstein, and R. H. Colby, *Macromolecules* **24**, 4701 (1991).
- [22] S. Tang, M. Wang, and B. D. Olsen, *J. Am. Chem. Soc.* **137**, 3946 (2015).
- [23] I. Mahmud Rasid, N. Holten-Andersen, and B. D. Olsen, *Macromolecules* **54**, 1354 (2021).
- [24] K. E. Feldman, M. J. Kade, E. W. Meijer, C. J. Hawker, and E. J. Kramer, *Macromolecules* **42**, 9072 (2009).
- [25] W. Shen, K. Zhang, J. A. Kornfield, and D. A. Tirrell, *Nat. Mater.* **5**, 153 (2006).
- [26] A. N. Semenov and M. Rubinstein, *Macromolecules* **31**, 1373 (1998).
- [27] L. G. Baxandall, *Macromolecules* **22**, 1982 (1989).
- [28] M. Rubinstein and A. N. Semenov, *Macromolecules* **34**, 1058 (2001).
- [29] S. Tang, A. Habicht, S. Li, S. Seiffert, and B. D. Olsen, *Macromolecules* **49**, 5599 (2016).
- [30] J. Ramirez, T. J. Dursch, and B. D. Olsen, *Macromolecules* **51**, 2517 (2018).
- [31] M. Shibayama, T. Norisuye, and S. Nomura, *Macromolecules* **29**, 8746 (1996).
- [32] S. Koizumi, M. Monkenbusch, D. Richter, D. Schwahn, and B. Farago, *J. Chem. Phys.* **121**, 12721 (2004).
- [33] M. Shibayama, Y. Fujikawa, and S. Nomura, *Macromolecules* **29**, 6535 (1996).
- [34] T. Tanaka, L. O. Hocker, and G. B. Benedek, *J. Chem. Phys.* **59**, 5160 (1973).
- [35] T. Kanaya, N. Takahashi, H. Takeshita, M. Ohkura, K. Nishida, and K. Kaji, *Polym. J.* **44**, 83 (2012).
- [36] T. Hiroi, M. Ohl, T. Sakai, and M. Shibayama, *Macromolecules* **47**, 763 (2014).
- [37] P. G. De Gennes, *Scaling Concepts in Polymer Physics* (Cornell University Press, Ithaca, NY, 1979).
- [38] M. Doi and S. F. Edwards, *The Theory of Polymer Dynamics* (Clarendon Press, Oxford, 1988).
- [39] R. Pecora, *Dynamic Light Scattering: Applications of Photon Correlation Spectroscopy* (Plenum Press, New York, 1985).
- [40] D. Richter, M. Monkenbusch, A. Arbe, and J. Colmenero, *Neutron Spin Echo in Polymer Systems*, Advances in Polymer Science Vol. 174 (Springer, Berlin, 2005).
- [41] M. Shibayama, *Bull. Chem. Soc. Jpn.* **79**, 1799 (2006).
- [42] S. Seiffert, *Prog. Polym. Sci.* **66**, 1 (2017).
- [43] M. Fernández-García, J. J. Martínez, and E. L. Madruga, *Polym. Commun.* **39**, 991 (1998).
- [44] A. M. Hecht, F. Horkay, P. Schleger, and E. Geissler, *Macromolecules* **35**, 8552 (2002).
- [45] H. Oikawa and H. Nakanishi, *Polymer* **34**, 3358 (1993).
- [46] M. Shibayama, Y. Shirotani, and Y. Shiwa, *J. Chem. Phys.* **112**, 442 (2000).

- [47] R. Liu and W. Oppermann, *Macromolecules* **39**, 4159 (2006).
- [48] T. Norisuye, Q. Tran-Cong-Miyata, and M. Shibayama, *Macromolecules* **37**, 2944 (2004).
- [49] T. Kanaya, N. Takahashi, K. Nishida, H. Seto, M. Nagao, and Y. Takeba, *Phys. B (Amsterdam)* **385-386**, 676 (2006).
- [50] L. Fang and W. Brown, *Macromolecules* **23**, 3284 (1990).
- [51] T. Kanaya, N. Takahashi, K. Nishida, H. Seto, M. Nagao, and T. Takeda, *Phys. Rev. E* **71**, 011801 (2005).
- [52] W. A. Petka, J. L. Harde, K. P. McGrath, D. Wirtz, D. A. Tirrell, J. L. Harden, K. P. McGrath, D. Wirtz, and D. A. Tirrell, *Science* **281**, 389 (1998).
- [53] B. D. Olsen, J. A. Kornfield, and D. A. Tirrell, *Macromolecules* **43**, 9094 (2010).
- [54] M. J. Glassman, J. Chan, and B. D. Olsen, *Adv. Funct. Mater.* **23**, 1182 (2013).
- [55] See Supplemental Material at <http://link.aps.org/supplemental/10.1103/PhysRevMaterials.7.075602> for the sodium dodecyl sulfate polyacrylamide gel electrophoresis (SDS PAGE) gels of purified proteins; SANS patterns and fits; NSE fitting; shear rheology plots; PFG NMR spectra and analysis; Monte Carlo bootstrapping of SANS and NSE data; calculation of the theoretical junction spacing. The Supplemental Material also contains Refs. [56–72].
- [56] S. P. O. Danielsen, B. J. Thompson, G. H. Fredrickson, T. Q. Nguyen, G. C. Bazan, and R. A. Segalman, *Macromolecules* **55**, 3437 (2022).
- [57] F. Horkay and B. Hammouda, *Colloid Polym. Sci.* **286**, 611 (2008).
- [58] A. Lerch, F. Käfer, S. Prévost, S. Agarwal, and M. Karg, *Macromolecules* **54**, 7632 (2021).
- [59] Z. K. Zander, G. Hua, C. G. Wiener, B. D. Vogt, and M. L. Becker, *Adv. Mater.* **27**, 6283 (2015).
- [60] M. Shibayama, T. Tanaka, and C. C. Han, *J. Chem. Phys.* **97**, 6829 (1992).
- [61] S. B. Kennedy, K. Littrell, P. Thiyagarajan, D. A. Tirrell, and T. P. Russell, *Macromolecules* **38**, 7470 (2005).
- [62] C. E. R. Edwards, D. J. Mai, S. Tang, and B. D. Olsen, *Phys. Rev. Mater.* **4**, 35 (2020).
- [63] T. Matsunaga, T. Sakai, Y. Akagi, U. Il Chung, and M. Shibayama, *Macromolecules* **42**, 1344 (2009).
- [64] T. Matsunaga, T. Sakai, Y. Akagi, U. Il Chung, and M. Shibayama, *Macromolecules* **42**, 6245 (2009).
- [65] I. Mahmud Rasid, C. Do, N. Holten-Andersen, and B. D. Olsen, *Soft Matter* **17**, 8960 (2021).
- [66] W. Shen, J. A. Kornfield, and D. A. Tirrell, *Soft Matter* **3**, 99 (2007).
- [67] T. Kanaya, M. Ohkura, K. Kaji, M. Furusaka, and M. Misawa, *Macromolecules* **27**, 5609 (1994).
- [68] F. Horkay, A. M. Hecht, S. Mallam, E. Geissler, and A. R. Rennie, *Macromolecules* **24**, 2896 (1991).
- [69] R.-J. Roe, *Methods of X-Ray and Neutron Scattering in Polymer Science* (Oxford University Press, Oxford, 2000).
- [70] M. Shibayama, M. Tsujimoto, and F. Ikkai, *Macromolecules* **33**, 7868 (2000).
- [71] F. Ikkai and M. Shibayama, *Phys. Rev. Lett.* **82**, 4946 (1999).
- [72] R. Navarro Pérez, J. E. Amaro, and E. Ruiz Arriola, *Phys. Lett. B* **738**, 155 (2014).
- [73] W. T. Heller, J. Hetrick, J. Bilheux, J. M. B. Calvo, W.-R. Chen, L. DeBeer-Schmitt, C. Do, M. Doucet, M. R. Fitzsimmons, W. F. Godoy, G. E. Granroth, S. Hahn, L. He, F. Islam, J. Lin, K. C. Littrell, M. McDonnell, J. McGaha, P. F. Peterson, S. V. Pingali *et al.*, *SoftwareX* **19**, 101101 (2022).
- [74] V. N. Malashkevich, R. A. Kammerer, V. P. Efimov, T. Schulthess, and J. Engel, *Science* **274**, 761 (1996).
- [75] S. C. Grindy, R. Learsch, D. Mozhdzhi, J. Cheng, D. G. Barrett, Z. Guan, P. B. Messersmith, and N. Holten-Andersen, *Nat. Mater.* **14**, 1210 (2015).
- [76] A. J. Peters and T. P. Lodge, *Macromolecules* **49**, 7340 (2016).
- [77] H. K. Beech, J. A. Johnson, and B. D. Olsen, *ACS Macro Lett.* **12**, 325 (2023).
- [78] S. Maccarrone, C. Scherzinger, O. Holderer, P. Lindner, M. Sharp, W. Richtering, and D. Richter, *Macromolecules* **47**, 5982 (2014).
- [79] A. Ghavami, H. Kobayashi, and R. G. Winkler, *J. Chem. Phys.* **145**, 1 (2016).
- [80] S. Maccarrone, A. Ghavami, O. Holderer, C. Scherzinger, P. Lindner, W. Richtering, D. Richter, and R. G. Winkler, *Macromolecules* **49**, 3608 (2016).
- [81] F. Roosen-Runge, M. Hennig, F. Zhang, R. M. J. Jacobs, M. Sztucki, H. Schober, T. Seydel, and F. Schreiber, *Proc. Natl. Acad. Sci. USA* **108**, 11815 (2011).
- [82] T. Ando and J. Skolnick, *Proc. Natl. Acad. Sci. USA* **107**, 18457 (2010).
- [83] J. Witte, T. Kyrey, J. Lutzki, A. M. Dahl, J. Houston, A. Radulescu, V. Pipich, L. Stingaciu, M. Kühnhammer, M. U. Witt, R. Von Klitzing, O. Holderer, and S. Wellert, *Soft Matter* **15**, 1053 (2019).
- [84] R. Oeser, B. Ewen, D. Richter, and B. Farago, *Phys. Rev. Lett.* **60**, 1041 (1988).
- [85] R. Wang, A. Alexander-Katz, J. A. Johnson, and B. D. Olsen, *Phys. Rev. Lett.* **116**, 188302 (2016).